Chinese Journal of Chemical Engineering 89 (2026) 187–197

Contents lists available at ScienceDirect

Chinese Journal of Chemical Engineering

journal homepage: www.elsevier.com/locate/CJChE

Full Length Article

Mass transfer and kinetic behavior studies on cycloaddition of carbon dioxide with propylene oxide catalyzed by ionic liquid in microchannel reactor

Yiqian Yang [1, 2], Yu Chen [2], Gang Wang [2], Hanwen Yan [2], Lili Wang [1, *], Shuguang Xiang [1], Chunshan Li [2, *]

[1] Institute of Process Systems Engineering, College of Chemical Engineering, Qingdao University of Science and Technology, Qingdao 266042, China
[2] State Key Laboratory of Mesoscience and Engineering, CAS Key Laboratory of Green Process and Engineering, Beijing Key Laboratory of Solid-State Battery and Energy Storage Process, Institute of Process Engineering, Chinese Academy of Sciences, Beijing 100190, China

ARTICLE INFO

Article history:
Received 13 July 2025
Received in revised form
30 July 2025
Accepted 30 July 2025
Available online 20 September 2025

Keywords:
CO_2 cycloaddition
Ionic liquid
Microchannel reactor
Mass transfer
Kinetic model

ABSTRACT

The synthesis of propylene carbonate (PC) from CO_2 and propylene oxide (PO) is a typical gas-liquid biphasic system, where gas-liquid mass transfer efficiency significantly influences CO_2 cycloaddition reactions. Here, we proposed a microchannel reaction system for the CO_2 cycloaddition reaction catalyzed by ionic liquid within an aqueous environment. The effect of liquid flow rate, temperature and residence time on gas-liquid flow pattern, catalytic performance and mass transfer were systematically investigated. The results revealed that the PC generation rate reached 560.11 $mmol \cdot ml^{-1} \cdot h^{-1}$) at a 50 cm of flow distance under reaction conditions of 105 °C, 2.5 MPa, Q_G = 176 $ml \cdot min^{-1}$ and Q_L = 0.3 $ml \cdot min^{-1}$. Variations in mass transfer rate and reaction rate at different flow distances were experimentally studied. The reaction efficiency gradually decreased with increasing flow distance, which were attributed to the reduction of mass transfer caused by decreasing bubble velocity. Optimizing bubble velocity at an appropriate position enhanced reaction efficiency by improving mass transfer, achieving a 97.7% PC yield within 2.85 min. Furthermore, a kinetic model coupling intrinsic kinetics with gas-liquid mass transfer was developed for CO_2 cycloaddition reaction. The kinetic model was applied to predict PC reaction rates in microchannel reactors at various temperatures and liquid flow rates, achieving an average relative error of 9.6%.

1. Introduction

Driven by fossil fuel reliance and escalating deforestation, atmospheric CO_2 concentration has risen from 0.028% in the 1750s to 0.042% in 2022 [1]. To mitigate CO_2 emissions' impact on global climate, nations worldwide have implemented carbon peaking and neutrality policies. Carbon capture, utilization and storage has been proposed to convert CO_2 into value-added products by utilizing it as a C1 resource, offering an alternative solution to curb excessive CO_2 emission [2,3]. However, the high-value utilization of CO_2 faces significant challenges due to the kinetic and thermodynamic stability. Activating CO_2 with PO to form cyclic carbonate is widely regarded as an environmentally benign and cost-effective synthetic route [4,5]. Cyclic carbonates are important chemical compounds, extensively used in synthesizing biocompatible polymers, serving as electrolytes in lithium-ion batteries, and functioning as aprotic solvents [6].

The synthesis of cyclic carbonate primarily depends on the ring-opening reaction of epoxides. A key limitation of the cycloaddition reaction between CO_2 and PO include the requirement for severe reaction conditions (180–200 °C, 5–8 MPa) [7,8]. With improved understanding of the mechanism involving nucleophile-promoted epoxide ring-opening, various catalytic systems have been developed, including metal-organic frameworks [9–11], deep eutectic solvents [12,13], organic catalysts [14], and ionic liquids [15,16]. Ionic liquids (ILs) exhibit unique properties such as hydrogen-bonding interactions, tunable structures, adjustable acid-base polarity, and high CO_2 solubility, enabling simultaneous facilitation of epoxide ring-opening and enhancing CO_2 adsorption [17]. Guan *et al.* [18] designed a guanidine-based ionic liquid tethering —NH_2 groups, which possessed abundant Lewis acidic sites and hydrogen-bond donors synergized to activate the

* Corresponding authors.
E-mail addresses: liliw@qust.edu.cn (L. Wang), csli@ipe.ac.cn (C. Li).

https://doi.org/10.1016/j.cjche.2025.07.018

epoxide. This system achieved a 98.2% yield of chloropropene carbonate with 99.2% selectivity under optimized conditions (103.2 °C, 1.03 MPa, and 1.85 h). Cheng *et al.* [19] developed a heterogeneous catalyst with hydrogen bond donors and ionic liquids for CO_2 cycloaddition reaction, obtaining a 94% of PC yield at 105 °C, 2 MPa, and 3 h. The hydrogen-bond donor groups in ILs activate epoxides *via* oxygen-directed interactions, increasing the conversion efficiency by 20% compared to conventional ILs. Cao *et al.* [20] synthesized bifunctional protic ionic liquids (DBPIL) as single-component and metal-free catalysts for CO_2 cycloaddition reaction. The DBPIL catalyst showed a 92% yield of products within 6 h at 30 °C and 1 bar CO_2. Notably, PC synthesis *via* CO_2 cycloaddition reaction represents a typical gas-liquid biphasic system where catalytic performance is governed by both reaction kinetics and mass transfer limitations. Although most of ILs system shows a remarkable yield of cyclic carbonate, extended residence times are invariably required due to limited gas-liquid mass transfer efficiency. Thus, gas-liquid mass transfer is a key factor for the CO_2 cycloaddition reaction in batch reactors [21].

The emergence of microchannel reactors has provided new possibilities for the highly efficient catalytic synthesis of PC from CO_2. Owing to their outstanding mass transfer efficiency and high surface-area-to-volume ratio, microreactors facilitate intensified mixing of multiphase reactants in gas-liquid reaction systems, thereby increasing mass transfer rates under identical conditions and reducing residence time by up to 90% compared to conventional batch reactors [22–24]. Yue *et al.* [25] investigated hydrodynamics and mass transfer during CO_2 absorption in microchannels, reporting a mass transfer coefficient in the microchannel 10 times higher than that of in conventional devices. Wu *et al.* [26] developed a continuous-flow microreaction system for the highly efficient synthesis of PC catalyzed by [BMIM]Br within a short residence time at 140 °C and 3.0 MPa. Previous studies revealed that adjusting microchannel sizes significantly enhanced mass transfer rates, while the effect of diffusion limitations on the reaction rate still existed [27]. Moreover, the mass transfer process of the CO_2 cycloaddition reaction in microchannels needs to be systematically investigated, as it directly governs the competition between the mass transfer and reaction kinetics.

Herein, we present a continuous microchannel reactor for synthesis of propylene carbonate by cycloaddition reaction of CO_2 and PO. Flow pattern analysis using high-speed camera images revealed an obvious enhancement in mass transfer due to increased gas-liquid interfacial area. The effects of liquid flow rate, temperature and residence time on the gas-liquid flow pattern, catalytic performance and mass transfer were systematically investigated. The initial reaction rate was obtained in a batch reactor to determine the reaction orders and intrinsic activation energy. The developed kinetic model integrated mass transfer effects with intrinsic kinetics, predicting PC generation rate in microreactors under various operational conditions. The competition between mass transfer and reaction kinetics at different flow distance was systematically elucidated. We propose a modified microchannel design that enhanced mass transfer, thereby significantly improving reaction efficiency. Compared to the traditional microchannel reactor, the optimized system achieves a higher PC yield with about 50% shorter residence time.

2. Experimental

2.1. Chemical materials

1-Hexyl-3-methylimidazolium bromide ([HMIM]Br) with 99% purity was supplied by Shanghai Chengjie Co., Itd. Propylene oxide (PO), 1,2-propanediol, propylene carbonate (PC) and 1,4-dioxane with 99% purity were all purchased from Aladdin Industrial Co., Itd. Ethanol was supplied by Sinopharm Chemical Reagent Co., Itd. The CO_2 gas with 99.999% purity was provided by Beijing Beiwen Gas Factory. Deionized water was provided by the laboratory. All materials were used without any purification.

2.2. Experimental apparatus

The schematic of microchannel reactor system is shown in Fig. 1. The liquid phase, which was composed of [HMIM]Br, H_2O and PO at the certain molar ratio of 0.14/0.25/1, was delivered using a high-pressure liquid chromatography pump (CP-M305, CoMetro Technology). The flow rate ranged from 0.001 to 5 $ml \cdot min^{-1}$, and the operating pressure was 0–41 MPa. The gas flow was controlled by a gas flowmeter with a maximum flow rate of 200 $cm^3 \cdot min^{-1}$ (D07, Beijing Aurasky Electronics Co., Itd.). The gas-liquid phase flow was mixed in the T-shape micromixer (internal diameter 2.0 mm, 316 L) before entering the microchannel reactor (internal diameter 2.0 mm, 316 L). An oil bath was used to control and maintain the reaction temperature. To observe gas-liquid flow patterns, two 60 mm long transparent PFA tubes with an inner diameter of 2 mm were connected to both ends of microchannel. A high-speed camera (Lingyun, Itd.) with a resolution of 2336 × 700 pixels and a shutter speed of 50 fps (1 fps = 0.304 $m \cdot s^{-1}$) was employed for imaging.

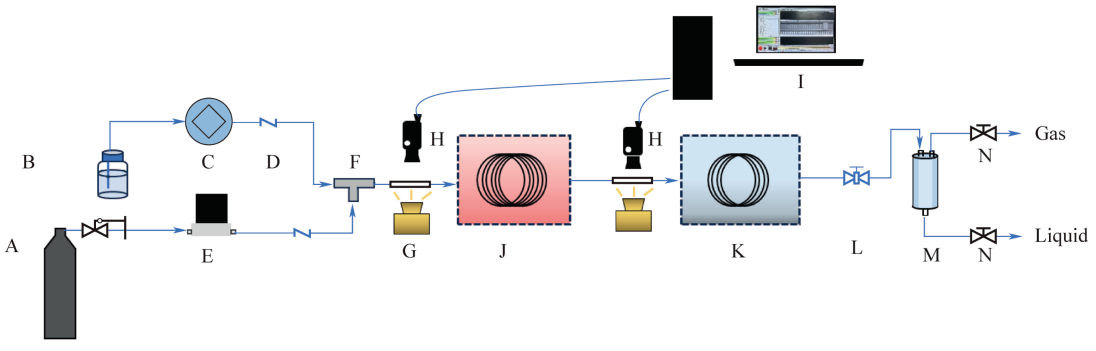

Fig. 1. Schematic of the experimental setup for the fixation of CO_2. A: CO_2 cylinder; B: liquid tank; C: constant-flow pump; D: one-way valve; E: mass flowmeter; F: T-shaped micromixer; G light source; H: high-speed camera; I: computer; J: spiral capillary in the oil bath; K: spiral capillary in the cold bath; L: back pressure valve; M; separator; N: needle valve.

The cold light source was positioned beneath the PFA tube to provide illumination. After stabilizing the flow system for 15 min, bubble length, bubble width, slug length, and liquid film thickness were captured. The flow patterns and mass transfer characteristics were determined based on the recorded images. The 316 L microchannel was connected after the end of the microchannel reactor to cool reactants. Finally, a gas-liquid separator collected liquid samples from the mixture after reaction completion.

2.3. Analysis methods

Liquid samples were analyzed by gas chromatography (GC, Shimadzu QP2010) equipped with BID detector and an SH-RTX-1 column (30 m × 0.53 mm × 3.00 μm) using the carrier gas of helium. 1,4-dioxane was selected as the internal standard. The chromatographic temperature program was as follows: The column temperature was initially set at 35 °C for 3 min, then increased at a rate of 5 °C·min^{-1} to 50 °C. The temperature was subsequently increased to 230 °C at 30 °C·min^{-1} and held at this final temperature.

The yield of PC was determined using the mass of the reactants and the final product collected within 20 min. To ensure the reliability and reproducibility of the experimental data, each experiment must be repeated at least three times.

The yields (Y) of PC and PG are calculated as follows:

$$Y_{PC} = \frac{n_{PC,1}}{n_{PO,0}} \times 100\% \quad (1)$$

$$Y_{PG} = \frac{n_{PG,1}}{n_{PO,0}} \times 100\% \quad (2)$$

The production rate of the PC was calculated using Eq. (3).

$$r_{PC} = \frac{C_{PC,1} - C_{PC,0}}{t} \quad (3)$$

The residence time in the microreactor was defined as

$$t = \frac{V_c}{Q_G + Q_L} = \frac{L_c \times \pi \times \frac{d_c^2}{4}}{Q_G + Q_L} \quad (4)$$

The gas bubble surface area and volume of Taylor unit were calculated using Eq. (5) and Eq. (6), respectively.

$$S = \pi \times d_B^2 + \pi \times d_B \times (L_B - d) \quad (5)$$

$$V_{Taylor} = (L_B + L_S) \times \pi \times \frac{d_c^2}{4} \quad (6)$$

The gas-liquid interfacial area (a) was determined by Eq. (7):

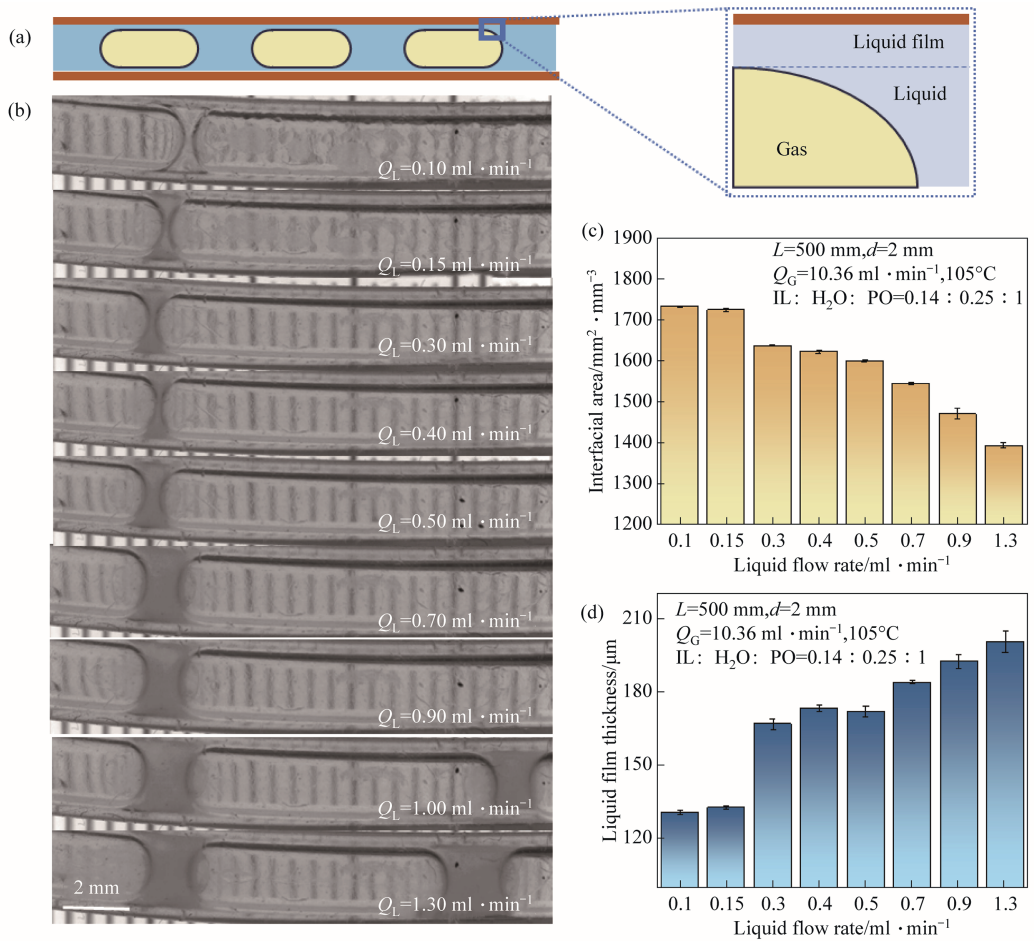

Fig. 2. Enhance mass transfer characteristics of CO_2 fixation in the microchannel reactor. (a) Schematic of the gas-liquid flow; (b) High-speed camera photographs of gas-liquid flow at various liquid flow rates in a 2 mm of transparent polypropylene tube. The gas flow and reactor temperature were fixed at 10.36 ml·min^{-1} and 105 °C; (c) Gas-interfacial area obtained from gas-liquid flow pattern at various liquid flow rates with an identical gas flow rate; (d) Thickness of the liquid film obtained from gas-liquid flow pattern at various liquid flow rates with an identical gas flow rate.

$$a = \frac{S}{V_{\text{Taylor}}} \tag{7}$$

The space-time yield (STY) of the components can be calculated by Eq. (8):

$$\text{STY} = \frac{M_{\text{PC}}}{M_{\text{cat}}\tau} \tag{8}$$

3. Results and Discussion

3.1. Gas-liquid Taylor flow formation in a microchannel reactor

The flow pattern plays a significant role in the stability and mass transfer performance of a microchannel reactor. The flow pattern was investigated at different liquid flow rates as recorded by a high-speed camera in transparent polypropylene tubes. Prior to entering the microchannel reactor, the reactant CO_2 and aqueous solution composed of [HMIM]Br, H_2O and PO with molar ratio of 0.14, 0.25 and 1 were mixed in a T-junction microdevice, leading to the formation of a Taylor flow (Fig. 2).

The Taylor flow pattern, which consists of gas bubbles, liquid slugs and liquid film thicknesses between the bubble and the microchannel wall, has been identified as a crucial factor for enhancing mass transfer due to its high gas-liquid interfacial area and stable internal circulation [28,29]. The effect of liquid flow rate on flow patterns and mass transfer characteristics (such as liquid film thickness and gas-liquid interfacial area) were investigated. When increasing the liquid flow rate from 0.10 to 1.30 ml·min^{-1} at a given gas flow rate of 10.36 ml·min^{-1}, 105 °C, and 2.5 MPa, the Taylor flow remained stable and the bubble length shortened (Fig. 2(b)), resulting in obviously reducing the gas-liquid interfacial area per Taylor unit (Fig. 2(c)) as calculated based on the dimensions of the gas and liquid phases in Taylor flow. The gas-liquid interfacial area in this system reached 1700 m^2·m^{-3}, substantially exceeding the ~600 m^2·m^{-3} typical of conventional bubble column reactors [30]. Liquid film thickness decreased with reducing liquid flow rate (Fig. 2(d)). The increase in the gas-liquid interfacial area and decrease in liquid film thickness were both beneficial for enhancing the diffusion of CO_2 molecules into the liquid phase [31].

The effect of reaction temperature on the gas-liquid flow patterns was also investigated in Fig. 3(a). When the reaction temperature ranged from 100°C to 115 °C, the flow patterns at the microreactor's outlet retained Taylor flow characteristics. Fig. 3(b) and (c) displayed the interfacial area and liquid film thickness at various reaction temperatures and liquid flow rates. Reducing liquid flow rate at a fixed temperature condition was beneficial to increasing the interfacial area per unit of volume and promoting the dissolution of CO_2 to the liquid phase [32].

3.2. CO_2 cycloaddition reaction in microchannel reaction

The evaluations of CO_2 cycloaddition reaction were carried out in a microchannel reactor (50 cm length) at 105 °C and 2.5 MPa. PC was the main product of CO_2 cycloaddition reaction under these reaction conditions. A small amount of propylene glycol (PG) was detected, which was primarily attributed to the hydrolysis of PO [33–35].

A series of CO_2 cycloaddition performances at different liquid flow rates was evaluated under a given gas flow rate of 10.36 ml·min^{-1} (Fig. 4(a)). When the liquid flow rate (Q_L) decreased from 1.30 to 0.30 ml·min^{-1}, the PC generation rate increased significantly from 170.62 to 560.11 mmol·ml^{-1}·h^{-1}, which was attribute to the improvement in mass transfer, as evidenced by the increase in gas-liquid interfacial area and decrease in liquid film thickness (Fig. 2(c)-(d)). Nevertheless, the PC generation rate decreased to 401.73 mmol·ml^{-1}·h^{-1} as the liquid flow rate further decreased from 0.30 to 0.10 ml·min^{-1}. As evidenced by the trends in the yields of PC and PG at various liquid flow rates, the PC yield decreased while the PG yield exhibited a significant increase as the decrease in liquid flow rate within the same range mentioned above. The volcano-shaped variation in PC yield with increasing of liquid flow rate resulted

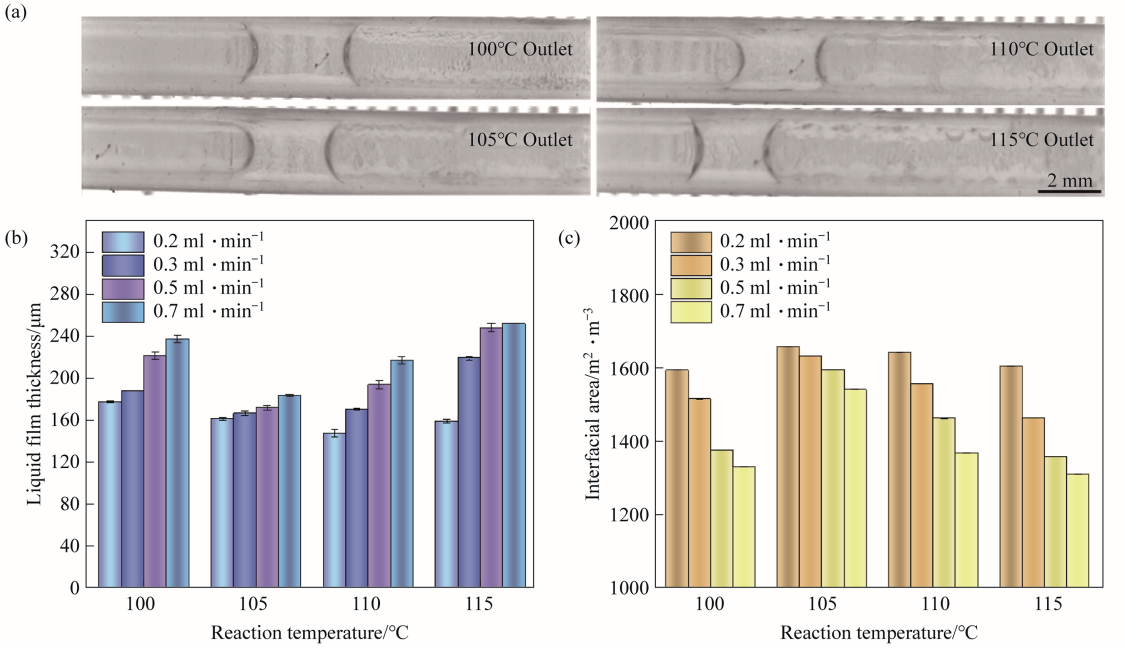

Fig. 3. (a) The flow pattern of gas-liquid in microchannels between inlet and outlet at various temperature. The gas flow rate and liquid flow rate were fixed at 10.36 ml·min^{-1} and 0.2 ml·min^{-1}; (b)-(c) The effect of liquid flow rate and reaction temperature on the liquid film thickness and gas-liquid interfacial area.

from the competition between mass transfer and reaction kinetics. Molecular dynamics simulations of the reaction system revealed the spatial distributions of [HMIM]Br, H_2O and PO, as shown in Fig. 5, with water exhibiting preferential colocalizations with [HMIM]Br (More detailed information about DFT calculation and molecular dynamics simulations was listed in Section S2 of the Supplementary Material). Quantitative binding energy calculations demonstrated stronger interactions for water-[HMIM]Br pairs (-8.46 kcal·mol^{-1}) compared to water-PO pairs (-3.54 kcal·mol^{-1}), further validating the distribution of [HMIM]Br and water. The concentration distribution of H_2O, [HMIM]Br and PO favored the generation of PC at high liquid flow rates and hardly no PG was generated. When the gas flow rate remained constant, the internal circulation in the liquid slug is enhanced with decreasing liquid flow rate, which may promote the hydrolysis of PO through more efficient water-PO contact (Fig. 5(d)) [36]. Fig. 4(b) shows the effect of ionic liquid concentration on the CO_2 cycloaddition reaction and PO hydrolysis at a liquid flow rate of 0.1 ml·min^{-1}. The experimental results conclusively validated the preceding analysis: PO hydrolysis was markedly suppressed with increasing ionic liquid concentration, as evidenced by a drastic decline in PG yield from 6.34% to 0.54%, while PC yield increased from 10.37% to 18.95%. It was further confirmed that the reaction transitioned from mass-transfer-limited to kinetics-controlled when Q_L was below 0.3 ml·min^{-1}.

The competition relationship between mass transfer and reaction kinetics is recognized as a significant factor in CO_2 cycloaddition reactions. Fig. 6(a) illustrated the catalytic performance of [HMIM]Br in the synthesis of PC from CO_2 and PO at various temperatures and liquid flow rates. The PC generation rate exhibited an obvious increase with higher reaction temperatures at a fixed liquid flow rate. A more than a doubling of the PC generation rate was observed with a 15 °C temperature rise at fixed Q_L. Furthermore, Fig. 6(b)-(e) displayed the effects of temperature and liquid flow rate on the yields of PC and PG. PO hydrolysis occurred at low liquid flow rates and the PG yield decreased with increasing reaction temperature. Notably, when the reaction temperature ranged from 100°C to 110 °C, a consistent trend was observed in the influence of liquid flow rate on the generation rate, where the PC generation rate first rose and subsequently declined with increasing liquid flow rates at the same reaction temperature. The reaction is governed by kinetic control at low flow rate (0.2 ml·min^{-1}) and transitions to mass transfer control at higher flow rate. When the reaction temperature was 115 °C, the

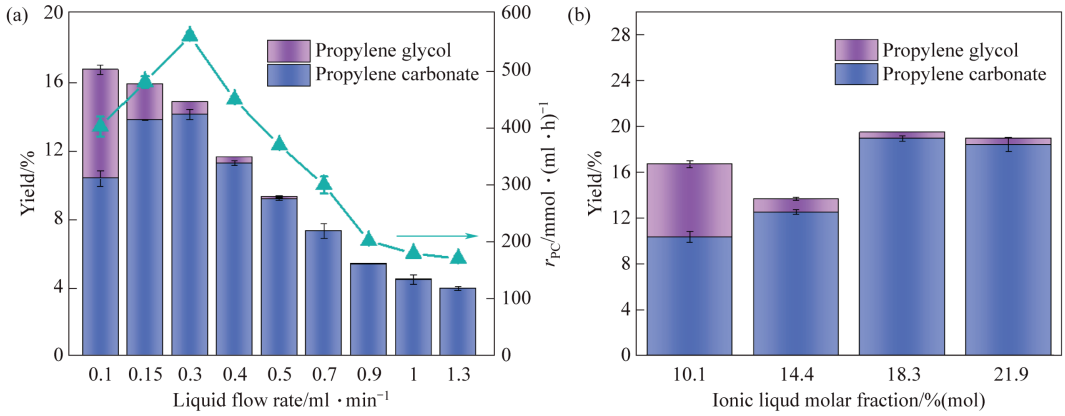

Fig. 4. (a) Product distributions and PC generation rate at various liquid flow rates; (b) The effect of ionic liquid molar fraction on the product distribution. (Q_G = 10.36 ml·min^{-1}).

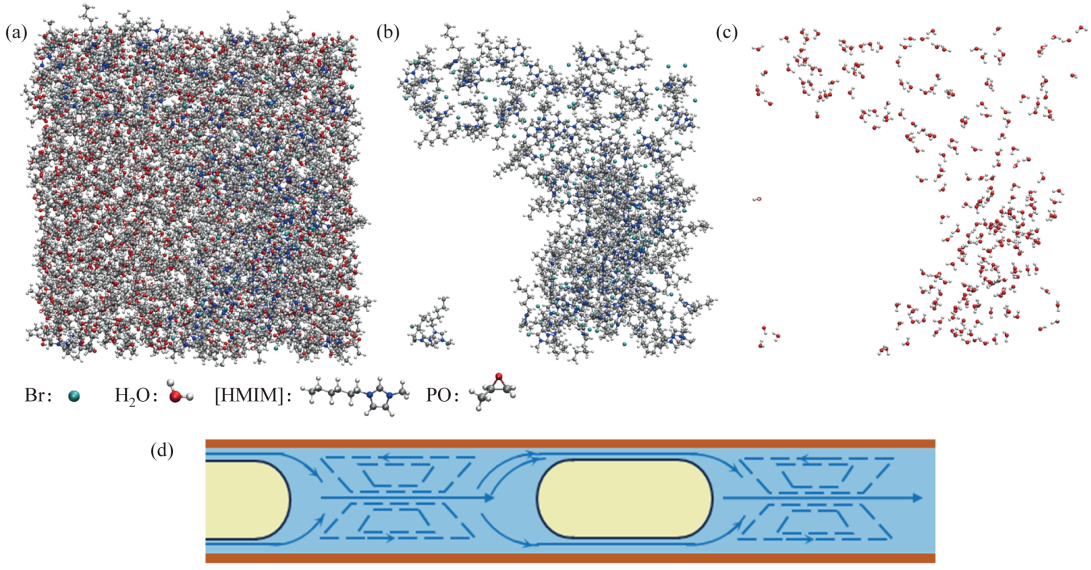

Fig. 5. (a)-(c) The DFT analysis for distribution of [HMIM]Br, H_2O and PO; (d) The schematic diagram of internal circulation in microchannels.

generation rate reached its maximum at the minimum liquid flow rate of 0.2 ml·min^{-1}, suggesting that the reaction rate dominated over the mass transfer rate at this temperature. The reaction transitioned from kinetic control to mass transfer control.

3.3. Kinetics studies

The rate equation for the CO_2 cycloaddition reaction catalyzed by [HMIM]Br can be formulated as follows [27]:

$$r = k[CO_2]^a[[HMIM]Br]^b[PO]^c \quad (9)$$

Where [PO], [CO_2] and [[HMIM]Br] represents the concentrations of PO, CO_2 and [HMIM]Br, and *a*, *b*, and *c* are the orders of reactions for PO, CO_2 and [HMIM]Br. In order to simplify the kinetic model, three assumptions were proposed based on the reaction mechanism [37–39]: (1) The concentration of the catalyst remained constant throughout the reaction; (2) The consumption of CO_2 concentration was constant due to a rapid equilibrium between CO_2 bubble in the microchannel and CO_2 which had been dissolved in the liquid phase; (3) The reaction was a pseudo-one-order reaction for PO. Eq. (9) can simplify to as follows:

$$r = -\frac{d[PO]}{dt} = k_{obs}[PO]^c \quad (10)$$

$$k_{obs} = k_o[CO_2]^a[HmimBr]^b \quad (11)$$

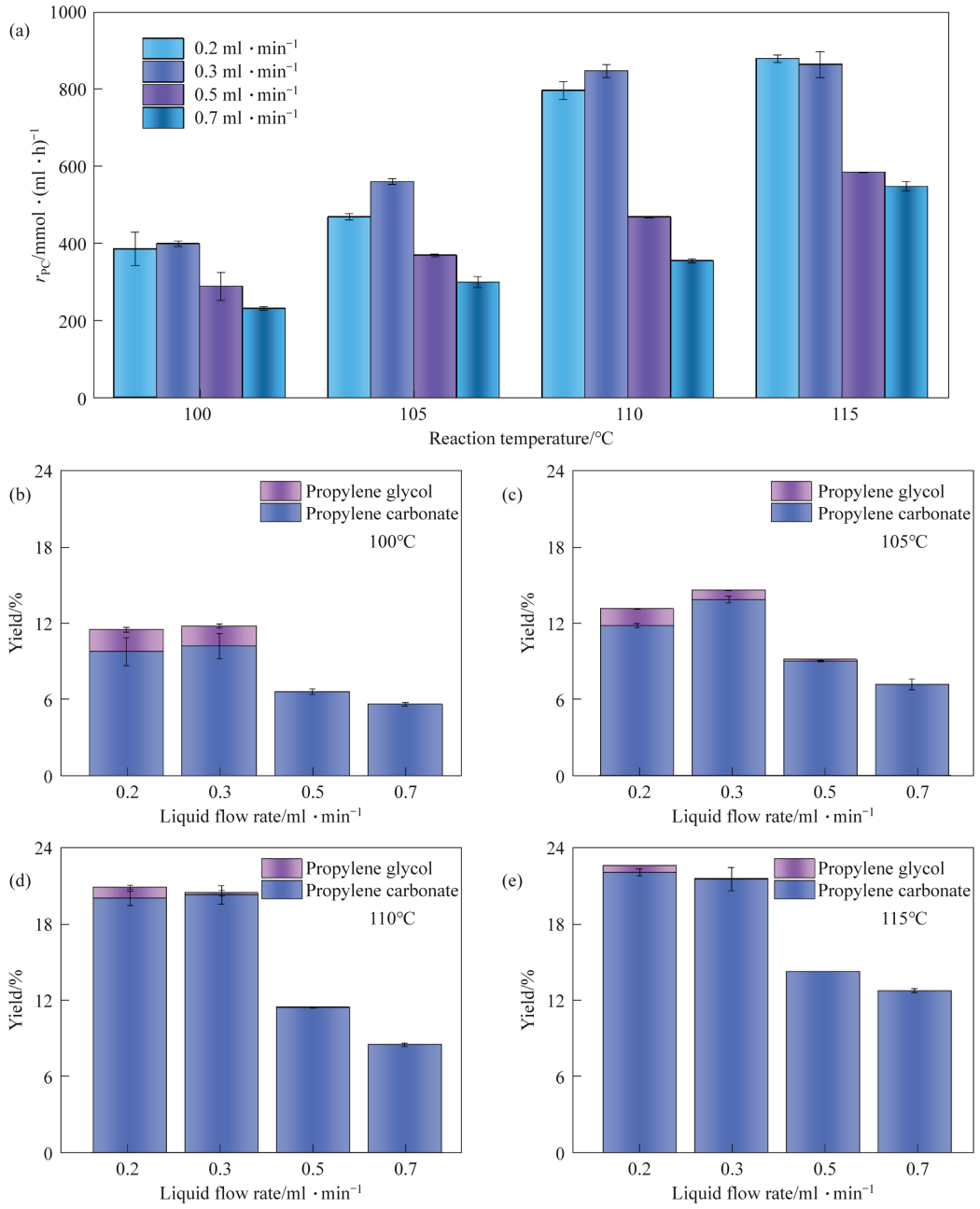

Fig. 6. The effect of liquid flow rate (a) and reaction temperature (b)-(d) on the PC generation rate and PC yield.

$$\ln\frac{[PO]}{[PO]_0} = -k_{obs} \times t + C \quad (12)$$

$$k_{obs} = A \times e^{\frac{-E_a}{RT}} \quad (13)$$

$$\ln k_{obs} = -\frac{E_a}{RT} + \ln A \quad (14)$$

In this section, the kinetics of CO_2 cycloaddition reaction were investigated in a batch reactor under operational conditions of 44–70 °C, 300–1100 r·min^{-1} and 2–3 MPa. Initially, the effect of residence time on the reaction rate was examined at 115 °C, 2.5 MPa and 700 r·min^{-1} (Fig. 7(a)). The linear relationship between ln[PO]/[PO]$_0$ and time based on Eq. (12) verified the pseudo-one-order assumption. To eliminate the effects of internal and external diffusion on the reaction rate, optimizations were performed for stirring rate, catalyst concentration, and reaction pressure. As presented in Fig. S1, the operating conditions were determined as 2.5 MPa, 10%(mol) and 700 r·min^{-1}. According to Eq. (11) and Eq. (13), the relationship between lnk_{obs} and 1/T was shown in Fig. 7(b). Temperature had a positive effect on the reaction rate, with the rate increasing as the increase in temperatures. The lnk_{obs} data exhibited a strong linear correlation with 1/T, and the regression coefficient exceeds 0.99. The activation energy was derived from the calculations as 75.82 kJ·mol^{-1}. According to the established kinetic model, a 15 °C increase in reaction temperature theoretically yielded a 2.57-fold enhancement in reaction rate. However, experimental observations of [HMIM]Br-catalyzed CO_2 cycloaddition in microchannel reactors demonstrated only a 2.16-fold rate increase under identical thermal conditions (as shown in Fig. 6(a)). Furthermore, the activation energy of [HMIM]Br is 62.55 kJ·mol^{-1} at the pressure of 2.5 MPa in the 2 mm microreactor [27]. The difference in activation energy and reaction rate indicated that the CO_2 cycloaddition reaction was limited by mass transfer in microchannel reactors.

In summary, the kinetic model for the cycloaddition reaction of CO_2 with PO catalyzed by [HMIM]Br to PC can be expressed by Eq. (15):

$$r = k_{obs}[PO] \quad (15)$$

Previous studies revealed that characteristics of hydrodynamics such as bubble length, liquid film thickness, and bubble velocity were strongly correlated with liquid flow rate, gas flow rate and k_La [40–43]. These parameters collectively determined the mass transfer efficiency between the gas and liquid phases, providing critical insights for optimizing mass transfer processes in microchannel reactors. Consequently, the model should be optimized by incorporating parameters that reflect mass transfer characteristics into the reaction kinetic model, where the $\left(\frac{n_L}{n_G}\right)^e$ and $\left(\frac{Q_L}{Q_G}\right)^f$ can be considered as the influence of hydrodynamics characteristics and mass transfer on the chemical reaction caused by flow rate change.

Eq. (13) and Eq. (15) can be reformulated as:

$$r = d\left(\frac{n_L}{n_G}\right)^e \left(\frac{Q_L}{Q_G}\right)^f e^{\frac{-E_a}{RT}} [PO] \quad (16)$$

Where d, e and f are fitting parameters. n_L/n_G is the molar ratio of PO and CO_2. Q_L and Q_G are the flow rate of liquid and gas, respectively. E_a is activation energy calculated by intrinsic kinetics, which is 75.82 kJ·mol^{-1}.

The parameters of Eq. (16) were determined based on the gas-liquid flow characteristics and reaction rates measured at 105 °C and different liquid flow rates. As shown in Fig. 8, the equation was subsequently applied to predict PC reaction rates under various temperatures and liquid flow rates, achieving an average relative error of 9.6%.

$$r = 8.62 \times 10^{10} \times \left(\frac{n_L}{n_G}\right)^{-0.2736} \times \left(\frac{Q_L}{Q_G}\right)^{-0.1804} \times e^{\frac{-75820}{RT}} \times [PO] \quad (17)$$

3.4. Variations in mass transfer rate and reaction rate along flow distances

Van Banten and Krishna developed a fundamental model for describing the mass transfer in Taylor bubble, which considered contributions of the caps at either end of the bubble and liquid film to mass transfer. The CFD simulations revealed that the film contribution was the major contribution to mass transfer. The concentration of CO_2 in the main body of the liquid phase can be considered negligible due to the rapid reaction kinetics between CO_2 and PO for cycloaddition reaction [27]. Luo, Scott and Shilimkan [44–46] employed a dimensionless empirical correlation for the determination of the liquid-side volumetric mass transfer coefficient (K_La) and

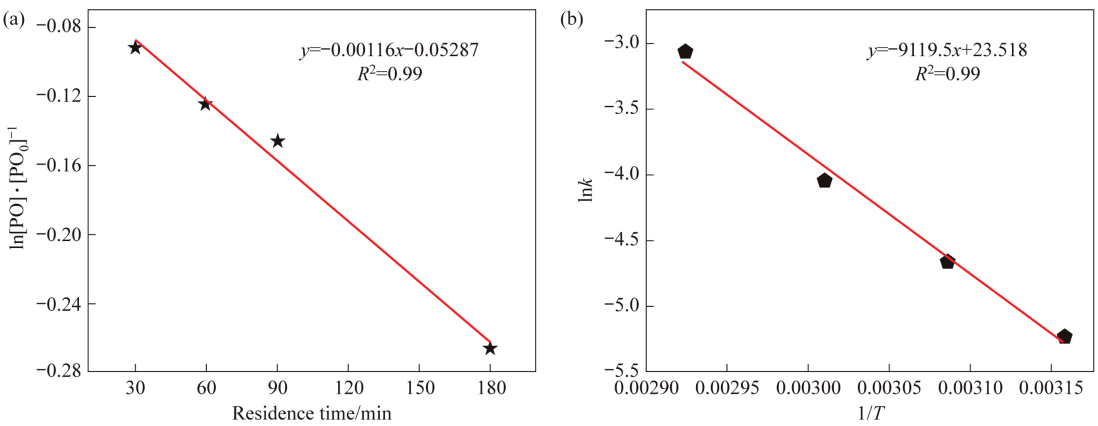

Fig. 7. (a) First order plot of [*PO*]/[*PO*$_0$] *versus* time in batch reactor; (b) Diagram of the Arrhenius curve of lnk_{obs} *versus* 1/T in batch reactor.

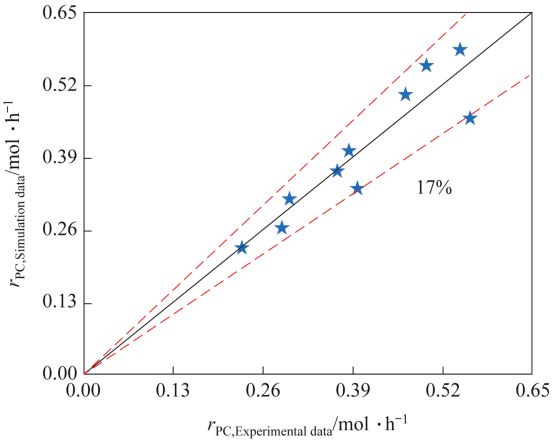

Fig. 8. Comparison between predicted and experimental data of PC reaction rate.

developed empirical correlations specific to different flow regimes. As for slug flow:

$$Sh_L \times a \times d_h = 0.084 \times Re_G^{0.213} \times Re_L^{0.937} \times Sc_L^{0.5} \quad (18)$$

Where *Re* and *Sc* are the Reynolds number and Schmidt number. The subscripts L and G stand for the liquid and gas, respectively. Eq. (18) can be reformulated as:

$$K_L \times a = 0.084 \times \left(\frac{\rho_G \times j_G}{\mu_G}\right)^{0.213} \times \left(\frac{\rho_L}{\mu_L}\right)^{0.437} \times j_L^{0.937} \times D_{CO_2}^{0.5} \times d_c^{-0.85} \quad (19)$$

For the liquid phase in this study, comprising water, propylene oxide, and ionic liquid, the concentrations of the ionic liquid had the most significant impact on the solubility of CO_2. Therefore, the dissolution of CO_2 in the other two components was neglected, and only its solubility in the ionic liquid was considered. C_1 was 0.38 mol L^{-1} calculated in the literature [27,47]. All the physical properties required for calculating Eq. (19) can be obtained through methods reported in the literature, experiments and Aspen simulations, such as D_{CO_2} and ρ_L (Section S3 in the Supplementary Material).

To analyze the mass transfer and kinetic characteristics of the process of synthesizing PC from CO_2 and PO catalyzed by [HMIM]Br, a comprehensive study was performed to analyze the changes in PO reaction rate, mass transfer rate, and Damköhler number (*Da*) during different flow distances under varying liquid flow rates. The introduction of the *Da* helped to clarify the dominant mechanisms in the reaction system [48].

$$Da = \frac{\text{mixing time}}{\text{reaction time}} = \frac{\text{reaction rate}}{\text{convective transport rate}} = \frac{k \times [PO]}{K_L \times a \times C_1} \quad (20)$$

To investigate the reaction process of PC synthesis in microchannels, a series of PC yield and PC generation rate at different

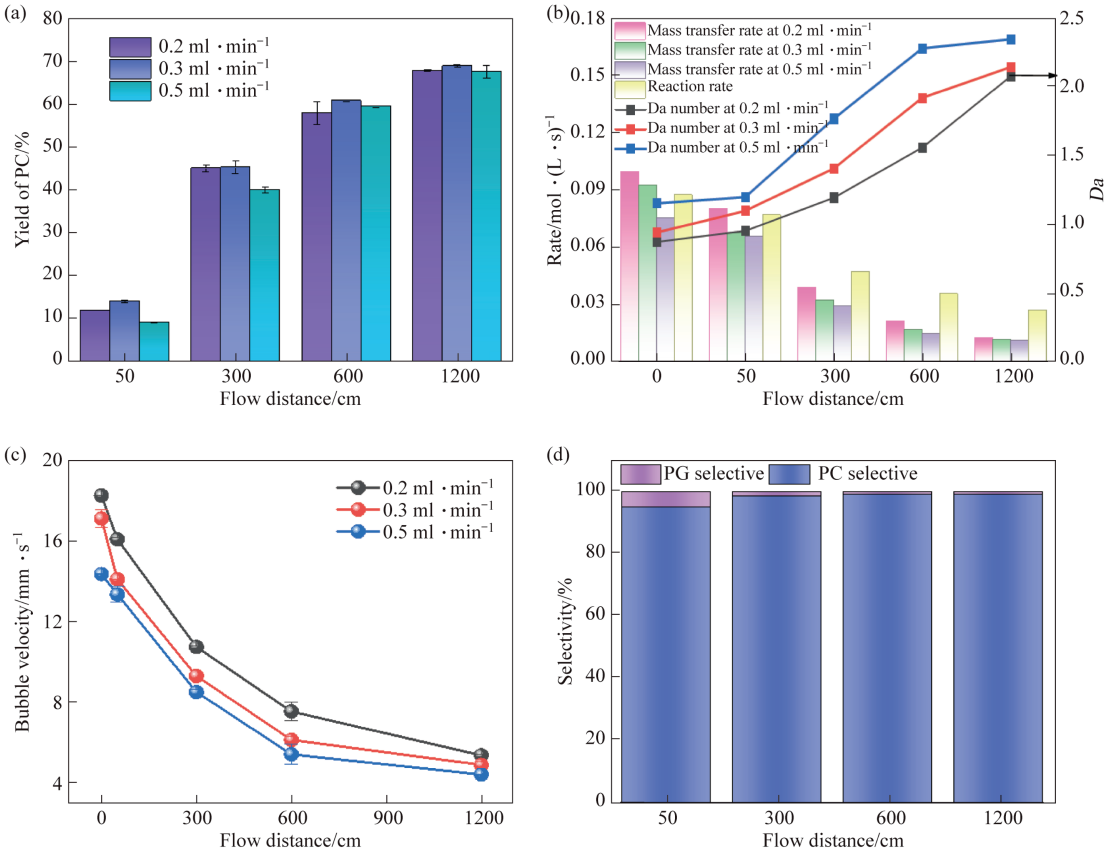

Fig. 9. (a) The yield of PC at various flow distances and liquid flow rates; (b) The variation of the Da at different flow distances and liquid flow rates; (c) The bubble flow velocity at different flow distance under the conditions of 105 °C, 2.5 MPa and gas flow rate of 176 cm^3·min^{-1}; (d) The selectivity of PC and PG at various flow distances (Q_L = 0.3 ml·min^{-1}).

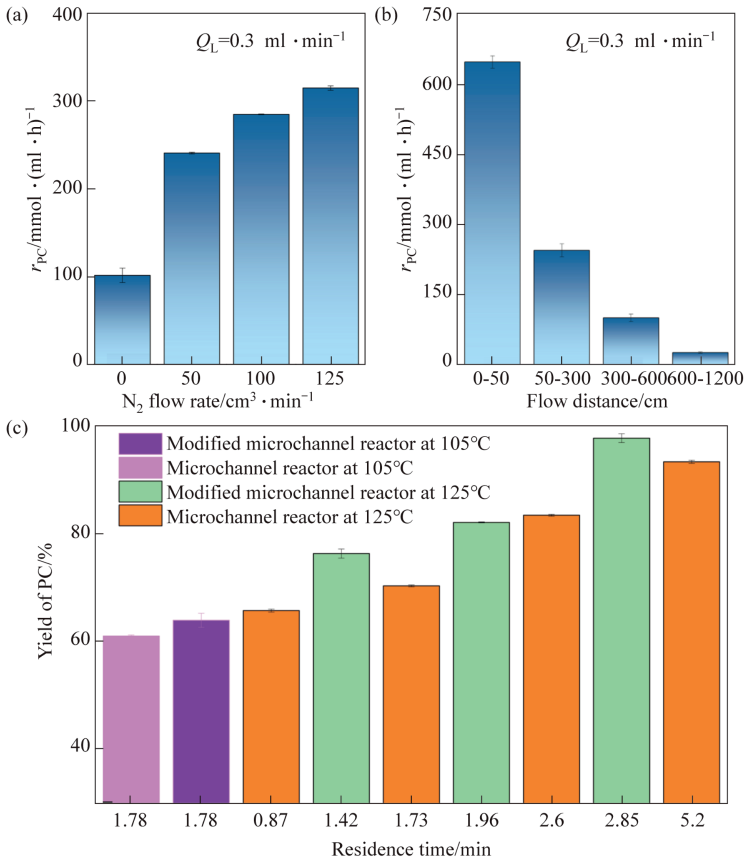

Fig. 10. (a) The effect of N_2 flow rate on the PC generation rate; (b) The PC generation rate. The reaction conditions were 105 °C, 2.5 MPa, CO_2 flow rate of 176 ml·min^{-1} and liquid flow rate of 0.3 ml·min^{-1}; (c) The yield of PC under different residence time and reaction conditions.

microchannel lengths was performed in the range of 30–1200 cm at 105 °C, 2.5 MPa and gas flow rate of 176 ml·min^{-1}. The results in Fig. 9(a) showed that the PC yield exhibited a maximum at the liquid flow rate of 0.3 ml·min^{-1}. The PC yield reached 14.1% at the microchannel length of 50 cm. When the microchannel length enlarged to 300 cm, the PC yield increased to 45.4%. Further extension of the microchannel to 600 cm resulted in a 15.5% PC yield improvement. However, the PC yield slightly increased at 8.1% across 600–1200 cm microchannel, demonstrating severe deterioration in reaction efficiency. Fig. 9(b) showed the variation of the *Da* during the reaction process at different liquid flow rates. The mass transfer rate increased with decreasing liquid flow rate and the calculated *Da* exhibited an obvious increase with the extension of the microchannel length.

The mass transfer rate showed a larger decline than that of reaction rater under different flow distance. The bubble velocity at various flow distances was obtained through high-speed camera. More than 200 images were captured for each set of experimental conditions, and the average value was used for further analysis. Fig. 9(c) displays that an approximate 50% reduction in bubble velocity at the 300 cm of flow distance. The decrease in bubble velocity adversely affected gas-liquid mass transfer, leading to an increase in the *Da* . The improvement of PC yield significantly decreased at flow distances exceeding 300 cm, primarily attributed to reduced mass transfer efficiency. As shown in Fig. 9(d), an increase in the microchannel length positively affected the PC selectivity. The PC selectivity exhibited a significant enhancement from 95.0% to 99.2% as the microchannel length extended from 50 cm to 1200 cm, which indicated that the concentration of PG declined progressively with extending residence time during PC production.

To investigate the effect of bubble velocity on the PC generation rate, a T-junction mixer was installed at the 300 cm position of the reactor to introduce nitrogen gas (non-reactive with PO) into the microchannel, effectively increasing bubble velocity and enhancing gas-liquid interfacial mass transfer. As shown in Fig. 10(a) and (b), the reaction efficiency at flow distances ranging from 300 to 600 cm

Table 1
Comparison of PC yield between modified microchannel reactor and state-of-art catalytic performances in literature [27].

Catalyst	Temperature/°C	Pressure/MPa	PC Yield/%	Residence time/min
PPh_3BuI/H_2O	125	2.0	97	60
[BMIM]Br	30	0.1	23	720
[BMIM]Cl	110	2.0	64	720
[HMIM]Br	120	1.5	94	120
$[EMIM]BF_4$	100	14.0	61	120
Multi-hydroxyl ILS	120	2.0	100	180
$[HMIM]Br/H_2O$	125	2.5	97.8	5.20
$[HMIM]Br/H_2O$	125	2.5	97.7	2.85

markedly increased due to introduction of N_2, which a 300% improvement in PC generation rate was achieved and the PC generation rate reached 314.6 mmol·ml^{-1}·h^{-1}. The results proved that increasing localized bubble velocity in microchannel reactor exerted a positive impact on reaction efficiency enhancement.

Fig. 10(c) displayed the PC yield at different residence time and different reaction conditions. The PC yield increased from 60.9% to 63.8% after modifying the microchannel reactor at 105 °C and 1.78 min. The increase in PC yield was more pronounced with increasing reaction temperature in the modified microchannel reactor, which the PC yield reached 97.7% at 125 °C and 2.85 min. Compared to the traditional microchannel reactor, the optimized system achieves a higher PC yield with about 50% shorter residence time, demonstrating significantly enhanced reaction efficiency (Table 1).

4. Conclusions

In this study, a continuous microchannel reactor was used for efficient synthesis of propylene carbonate *via* CO_2 cycloaddition reaction. The excellent catalytic activity can be attributed to significantly enhanced mass transport. The effects of liquid flow rate, temperature and residence time on the gas-liquid flow pattern, catalytic performance and mass transfer were systematically investigated. Analysis of the competition relationship between mass transfer and reaction kinetics at different flow distances revealed that increasing bubble velocity at an appropriate position enhances reaction efficiency by improving mass transfer, with the optimized system achieving a 97.7% PC yield with about 50% shorter residence time. Furthermore, the intrinsic kinetics for synthesizing PC by cycloaddition reaction of CO_2 and PO catalyzed by [HMIM]Br in the presence of water were determined in a batch reactor. The results illustrated that the reaction rate displayed a pseudo-one-order dependence on PO and active energy was 75.82 kJ·mol^{-1} calculated by the Arrhenius equation. The kinetic model should be optimized by incorporating parameters that reflected mass transfer and reaction kinetic characteristics. With an average relative error of 9.6%, the kinetic model demonstrated high reliability.

CRediT Authorship Contribution Statement

Yiqian Yang: Writing — original draft, Methodology, Investigation, Funding acquisition, Conceptualization. Yu Chen: Validation, Resources. Gang Wang: Writing — review & editing, Conceptualization. Hanwen Yan: Validation, Data curation. Lili Wang: Validation, Data curation, Conceptualization. Shuguang Xiang: Supervision, Conceptualization. Chunshan Li: Supervision, Project administration, Funding acquisition, Conceptualization.

Declaration of Competing Interest

The authors declare that they have no known competing financial interests or personal relationships that could have appeared to influence the work reported in this paper.

Acknowledgements

This work was supported by the National Key Projects for Fundamental Research and development of China (2020YFA0710202), the China Postdoctoral Science Foundation (2024M761567) and Shandong Postdoctoral Science Foundation (SDCX-ZG-202400271).

Supplementary Material

Supplementary data to this article can be found online at https://doi.org/10.1016/j.cjche.2025.07.018.

Nomenclature

A	pre-exponential factor
C_1	CO_2 concentration at the gas-liquid interface, mol·ml^{-1}
C_L	CO_2 concentration in the main body of the liquid phase, mol·ml^{-1}
C_{PC}	PC concentration, mol·ml^{-1}
Da	Damköhler number
D_{co_2}	diffusion coefficient of CO_2 in the liquid phase, m^2·s^{-1}
d_B	bubble diameter, m
d_c	microchannel diameter, m
E_a	activation energy, kJ·mol^{-1}
K_La	liquid-phase volume transfer coefficient, s^{-1}
K_L	liquid-phase transfer coefficient, m·s^{-1}
K_{obs}	reaction rate constant, min^{-1}
L_B	bubble length, m
L	microchannel length, m
L_S	liquid slug length, m
M	mass, g
N	mole number, mol
Q	flow rate, ml·min^{-1}
R	ideal gas constant (8.314 J·(mol·K) $^{-1}$)
S	bubble superficial area, m^2
Sh	Sherwood number
T	temperature, K
t	residence time, s
V_c	microchannel volume, m^3
V_{Taylor}	Taylor volume, m^3
α	gas-liquid interfacial area, mm^2·mm^{-3}
σ	liquid film thickness, mm
τ	residence time in microchannel reactor, min

References

[1] S.H. Wei, M.K. Albolkany, L. Zhao, B. Liu, Supramolecular chemistry for carbon dioxide capture, *Coord. Chem. Rev.* 535 (2025) 216655.
[2] S. Takeya, K.A. Udachin, I.L. Moudrakovski, R. Susilo, J.A. Ripmeester, Direct space methods for powder X-ray diffraction for guest-host materials: applications to cage occupancies and guest distributions in clathrate hydrates, *J. Am. Chem. Soc.* 132 (2) (2010) 524–531.
[3] H.P. Veluswamy, Energy storage in hydrates: status, recent trends, and future prospects, *ACS Appl. Energy Mater.* 7 (24) (2024) 11497–11515.
[4] R.C. Luo, X.Y. Liu, M. Chen, B.Y. Liu, Y.X. Fang, Recent advances on imidazolium-functionalized organic cationic polymers for CO_2 adsorption and simultaneous conversion into cyclic carbonates, *ChemSusChem* 13 (16) (2020) 3945–3966.
[5] J. Artz, T.E. Müller, K. Thenert, J. Kleinekorte, R. Meys, A. Sternberg, A. Bardow, W. Leitner, Sustainable conversion of carbon dioxide: an integrated review of catalysis and life cycle assessment, *Chem. Rev.* 118 (2) (2018) 434–504.
[6] T. Sakakura, J.C. Choi, H. Yasuda, Transformation of carbon dioxide, *Chem. Rev.* 107 (6) (2007) 2365–2387.
[7] E.A. Quadrelli, G. Centi, J.L. Duplan, S. Perathoner, Carbon dioxide recycling: emerging large-scale technologies with industrial potential, *ChemSusChem* 4 (9) (2011) 1194–1215.
[8] H. You, E.H. Wang, H. Cao, C.W. Zhuo, S.J. Liu, X.H. Wang, F.S. Wang, From impossible to possible: atom-economic polymerization of low strain five-membered carbonates, *Angew. Chem. Int. Ed.* 61 (5) (2022) e202113152.
[9] M.L. Ding, R.W. Flaig, H.L. Jiang, O.M. Yaghi, Carbon capture and conversion using metal–organic frameworks and MOF-based materials, *Chem. Soc. Rev.* 48 (10) (2019) 2783–2828.
[10] P.Z. Li, X.J. Wang, J. Liu, J.S. Lim, R.Q. Zou, Y.L. Zhao, A triazole-containing metal-organic framework as a highly effective and substrate size-dependent catalyst for CO_2 conversion, *J. Am. Chem. Soc.* 138 (7) (2016) 2142–2145.
[11] X.D. Lang, L.N. He, Green catalytic process for cyclic carbonate synthesis from carbon dioxide under mild conditions, *Chem. Rec.* 16 (3) (2016) 1337–1352.
[12] X.Q. Yang, Z.M. Liu, P. Chen, F. Liu, T.X. Zhao, Effective synthesis of cyclic carbonates from CO_2 and epoxides catalyzed by acetylcholine bromide-based deep eutectic solvents, *J. CO_2 Util.* 58 (2022) 101936.

[13] X.Q. Yang, Q.Z. Zou, T.X. Zhao, P. Chen, Z.M. Liu, F. Liu, Q. Lin, Deep eutectic solvents as efficient catalysts for fixation of CO_2 to cyclic carbonates at ambient temperature and pressure through synergetic catalysis, *ACS Sustainable Chem. Eng.* 9 (31) (2021) 10437−10443.
[14] Y. Xie, T.T. Wang, X.H. Liu, K. Zou, W.Q. Deng, Capture and conversion of CO_2 at ambient conditions by a conjugated microporous polymer, *Nat. Commun.* 4 (2013) 1960.
[15] K. Jasiak, A. Siewniak, K. Kopczyńska, A. Chrobok, S. Baj, Hydrogensulphate ionic liquids as an efficient catalyst for the synthesis of cyclic carbonates from carbon dioxide and epoxides, *J. Chem. Technol. Biotechnol.* 91 (11) (2016) 2827−2833.
[16] M.S. Liu, L. Liang, T. Liang, X.L. Lin, L. Shi, F.X. Wang, J.M. Sun, Cycloaddition of CO_2 and epoxides catalyzed by dicationic ionic liquids mediated metal halide: influence of the dication on catalytic activity, *J. Mol. Catal. Chem.* 408 (2015) 242−249.
[17] V.B. Saptal, B.M. Bhanage, Current advances in heterogeneous catalysts for the synthesis of cyclic carbonates from carbon dioxide, *Curr. Opin. Green Sustainable Chem.* 3 (2017) 1−10.
[18] N.J. Feng, L.Y. Cheng, Y.K. Zhang, Y.J. Tao, H. Wan, C. Chen, G.F. Guan, Multiple-site activation induced by guanidine ionic liquid decorated chromium (III) terephthalate for coupling of carbon dioxide with epoxides, *J. Colloid Interface Sci.* 687 (2025) 561−572.
[19] H.B. Gou, X.F. Ma, Q. Su, L. Liu, T. Ying, W. Qian, L. Dong, W.G. Cheng, Hydrogen bond donor functionalized poly(ionic liquid)s for efficient synergistic conversion of CO_2 to cyclic carbonates, *Phys. Chem. Chem. Phys.* 23 (3) (2021) 2005−2014.
[20] J.P. Cao, Y.S. Xue, N.F. Li, J.J. Gong, R.K. Kang, Y. Xu, Lewis acid dominant windmill-shaped V(8) clusters: a bifunctional heterogeneous catalyst for CO_2 cycloaddition and oxidation of sulfides, *J. Am. Chem. Soc.* 141 (49) (2019) 19487−19497.
[21] Y.C. Zhao, C.Q. Yao, G.W. Chen, Q. Yuan, Highly efficient synthesis of cyclic carbonate with CO_2 catalyzed by ionic liquid in a microreactor, *Green Chem.* 15 (2) (2013) 446−452.
[22] R. Gopi, V. Thangarasu, A. Vinayakaselvi M, A. Ramanathan, A critical review of recent advancements in continuous flow reactors and prominent integrated microreactors for biodiesel production, *Renew. Sustain. Energy Rev.* 154 (2022) 111869.
[23] P.L. Suryawanshi, S.P. Gumfekar, B.A. Bhanvase, S.H. Sonawane, M.S. Pimplapure, A review on microreactors: reactor fabrication, design, and cutting-edge applications, *Chem. Eng. Sci.* 189 (2018) 431−448.
[24] J.F. Ran, X.X. Wang, Y.H. Liu, S.H. Yin, S.W. Li, L.B. Zhang, Microreactor-based micro/nanomaterials: fabrication, advances, and outlook, *Mater. Horiz.* 10 (7) (2023) 2343−2372.
[25] J. Yue, G.W. Chen, Q. Yuan, L.G. Luo, Y. Gonthier, Hydrodynamics and mass transfer characteristics in gas−liquid flow through a rectangular microchannel, *Chem. Eng. Sci.* 62 (7) (2007) 2096−2108.
[26] Y.X. Wu, Y.C. Ding, J.H. Xu, Y.D. Wang, K. Mumford, G.W. Stevens, W.Y. Fei, Efficient fixation of CO_2 into propylene carbonate with [BMIM] Br in a continuous-flow microreaction system, *Green Energy Environ.* 6 (2) (2021) 291−297.
[27] Y. Chen, J.Y. Yu, Y.Q. Yang, F. Huo, C.S. Li, A continuous process for cyclic carbonate synthesis from CO_2 catalyzed by the ionic liquid in a microreactor system: reaction kinetics, mass transfer, and process optimization, *Chem. Eng. J.* 455 (2023) 140670.
[28] L. Sheng, Y.C. Chen, J. Deng, G.S. Luo, High-frequency formation of bubble with short length in a capillary embedded step T-junction microdevice, *AIChE J.* 67 (11) (2021) e17376.
[29] L. Sheng, Y.C. Chen, K. Wang, J. Deng, G.S. Luo, General rules of bubble formation in viscous liquids in a modified step T-junction microdevice, *Chem. Eng. Sci.* 239 (2021) 116621.
[30] J.C. Charpentier, Mass-transfer rates in gas-liquid absorbers and reactors, *Adv. Chem. Eng.* 11 (1981) 133. Elsevier.
[31] C.S. Li, H.C. Zhang, W.X. Liu, L. Sheng, M.J. Cheng, B.J. Xu, G.S. Luo, Q. Lu, Efficient conversion of propane in a microchannel reactor at ambient conditions, *Nat. Commun.* 15 (1) (2024) 884.
[32] Y.R. Yin, T.T. Fu, C.Y. Zhu, R.W. Guo, Y.G. Ma, H.Z. Li, Dynamics and mass transfer characteristics of CO_2 absorption into MEA/[Bmim] [BF_4] aqueous solutions in a microchannel, *Sep. Purif. Technol.* 210 (2019) 541−552.
[33] Y. Zhang, H. Hu, J. Ju, Q.Q. Yan, V. Arumugam, X.C. Jing, H.Q. Cai, Y.N. Gao, Ionization of a covalent organic framework for catalyzing the cycloaddition reaction between epoxides and carbon dioxide, *Chin. J. Catal.* 41 (3) (2020) 485−493.
[34] K. Kiatkittipong, M.A.A. Mohamad Shukri, W. Kiatkittipong, J.W. Lim, P.L. Show, M.K. Lam, S. Assabumrungrat, Green pathway in utilizing CO_2 *via* cycloaddition reaction with epoxide: a mini review, *Processes* 8 (5) (2020) 548.
[35] J. Sun, J.Y. Ren, S.J. Zhang, W.G. Cheng, Water as an efficient medium for the synthesis of cyclic carbonate, *Tetrahedron Lett.* 50 (4) (2009) 423−426.
[36] Y.Y. Chen, C.Y. Zhu, T.T. Fu, Y.G. Ma, Mass transfer enhancement of CO_2 absorption into [Bmim] [BF4] aqueous solution in microchannels by heart-shaped grooves, *Chem. Eng. Process. Process Intensif.* 167 (2021) 108536.
[37] Y.X. Wu, A. Chen, X.Y. Liu, J.H. Xu, Y.D. Wang, K. Mumford, G.W. Stevens, W.Y. Fei, Kinetic study of highly efficient CO_2 fixation into propylene carbonate using a continuous-flow reactor, *Chem. Eng. Process. Process Intensif.* 159 (2021) 108235.
[38] X. Jiang, F.L. Gou, C.Z. Qi, C_{2v}-symmetric metalloporphyrin promoted cycloaddition of epoxides with CO_2 under atmospheric pressure, *J. CO_2 Util.* 29 (2019) 134−139.
[39] R.C. Luo, W.Y. Zhang, Z. Yang, X.T. Zhou, H.B. Ji, Synthesis of cyclic carbonates from epoxides over bifunctional salen aluminum oligomers as a CO_2-philic catalyst: catalytic and kinetic investigation, *J. CO_2 Util.* 19 (2017) 257−265.
[40] C.Q. Yao, Y.C. Zhao, J. Zheng, Q. Zhang, G.W. Chen, The effect of liquid viscosity and modeling of mass transfer in gas−liquid slug flow in a rectangular microchannel, *AIChE J.* 66 (5) (2020) e16934.
[41] G. Berčič, A. Pintar, The role of gas bubbles and liquid slug lengths on mass transport in the Taylor flow through capillaries, *Chem. Eng. Sci.* 52 (21−22) (1997) 3709−3719.
[42] J.M. van Baten, R. Krishna, CFD simulations of mass transfer from Taylor bubbles rising in circular capillaries, *Chem. Eng. Sci.* 59 (12) (2004) 2535−2545.
[43] C.Q. Yao, Y.C. Zhao, G.W. Chen, Multiphase processes with ionic liquids in microreactors: hydrodysnamics, mass transfer and applications, *Chem. Eng. Sci.* 189 (2018) 340−359.
[44] D. Luo, S.M. Ghiaasiaan, Liquid-side interphase mass transfer in cocurrent vertical two-phase channel flows, *Int. J. Heat Mass Tran.* 40 (3) (1997) 641−655.
[45] D.S. Scott, W. Hayduk, Gas absorption in horizontal cocurrent bubble flow, *Can. J. Chem. Eng.* 44 (3) (1966) 130−136.
[46] R.V. Shilimkan, J.B. Stepanek, Effect of tube size on liquid side mass transfer in co-current gas-liquid upward flow, *Chem. Eng. Sci.* 32 (11) (1977) 1397−1400.
[47] A. Muhammad, A. Shafeeq, Z. ul Hasan Rizvi, A. Ijaz, M.I. Abdul Mutalib, Experimental solubility of CO_2 and CH_4 in imidazolium based ionic liquid; [C_6mim] [BF_4] at high pressures. 2010 2nd International Conference on Chemical, Biological and Environmental Engineering, IEEE, Cairo, 2010, pp. 39−42.
[48] G.K. Patterson, E.L. Paul, S.M. Kresta, A.W. Etchells Iii, Mixing and chemical reactions, in: Handbook of Industrial Mixing, John Wiley & Sons Inc, 2003.